Available online at www.sciencedirect.com

ScienceDirect

ARTICLE

Preparation and Characterization of Boron-Doped Nanodiamond

Yan Xianrong[1],   Li Xiaojie[1,2],   Wang Xiaohong[1,2],   Yan Honghao[1,2]

[1] Dalian University of Technology, Dalian 116024, China; [2] State Key Laboratory of Structural Analysis for Industrial Equipment, Dalian 116024, China

Abstract: Boron-doped nanodiamond was prepared by a high-temperature vacuum-diffusion method. Thermogravimetric analysis, X-ray photoelectron spectroscopy, X-ray diffraction (XRD), Fourier-transform infrared spectroscopy, Raman spectroscopy, and transmission electron microscopy were used to characterize the prepared material. Results show that the product mainly contains C, O, and B in mass fractions of 92.08%, 7.14%, and 0.78%, respectively. In addition to diamond $(111)_D$ and $(220)_D$ diffraction peaks, hexagonal diamond $(100)_D$ diffraction peaks are also observed in the XRD pattern of the boron-doped product. The introduction of B atoms increases the defect content in the nanodiamond and causes the Raman G peak to move to 1620 cm^{-1}. B atoms are mainly present in two forms in the diamond lattice: substitutional carbon atoms in C-B bonds, and being bonded with impurity elements (such as B-O). The shape and morphology of the boron-doped nanodiamond particles (particle size of detonation nanodiamond, 2~10 nm) exhibit no obvious changes compared to the pristine nanodiamond. However, a small amount of cubic diamond is observed. In conclusion, the initial oxidation temperature of the boron-doped nanodiamond increases by 175 °C, the oxidation rate is slower, and the thermal stability is improved.

Key words: boron-doped nanodiamond; oxidation resistance; thermal stability; high temperature vacuum diffusion method

Boron-doped diamond (IIb-type) exhibits many attractive properties, including high oxidation and impact resistance, excellent chemical stability, and semiconducting features[1]. The incorporation of boron oxide affects nanodiamond's properties, including the crystal morphology and quality, which are important factors to control for device applications.

Boron-doped diamond has attracted significant research interest[1,2]. Gheeraert investigated the amount of diborane needed to improve the crystalline quality of deposited diamond by studying changes in Raman spectral features[3]. A clear increase in the compressive component of the residual stress as a function of the doping level was observed for B/C ratios higher than 10^{-2} [4]. The dopant level also influenced the lattice parameters at a B/C ratio of 2×10^{-2}. The expansion of the lattice parameters has been attributed to compressive thermal stress in the diamond films[5,6]. Kaner[7] studied the influence of boron on the oxidation properties of doped carbon

fibers. The boron-derived protection of diamond against oxidation has been attributed to the formation of boron oxide, electron transfer, and the inhibition of CO[8].

Boron doping in diamond films is usually accomplished via chemical vapor deposition (CVD) during diamond growth or by ion implantation after growth[9,10]. In the present paper, boron atoms were deposited on the nanodiamond surface by vacuum diffusion. The boron-doped diamond was then prepared at elevated temperature under a protective atmosphere (such as He or Ar) to prevent oxidation of the nanodiamond. The product was studied by X-ray diffraction (XRD), X-ray photoelectron spectroscopy (XPS), Raman spectroscopy, Fourier-transform infrared spectroscopy (FTIR), transmission electron microscopy (TEM), and thermogravimetric analysis (TGA). The oxidation resistance and thermal stability of the boron-doped product were clearly improved, as confirmed thermogravimetrically. These improved characteristics may allow a broader range for

boron-doped nanodiamond in microelectronic[11] and electro-chemical[12] applications.

1 Experiment

The diamond particles and carbide elements (such as titanium, tungsten, boron, silicon, and chromium) were evenly mixed at specific temperatures in a vacuum environment, and a coating layer formed on the diamond surface. If the carbide powder was used directly, the mixture was easy to sinter at the reaction temperature and was unfavorable to subsequent processing. An improved effective method uses the oxidation forms of the carbonization elements (such as boron oxide, silicon oxide, or chromium oxide). In the case of boron oxide, excess reagent can be conveniently removed by water washing after the reaction. Ion transfer during carbonization depends greatly on the flow of gas and the diffusion of the solid powder. Carbon atoms coat the diamond surface through vertical migration of species such as CO formed from the surface carbon atoms and the oxide or oxygen atoms from oxide decomposition. CO can not only loosen the nanodiamond and carbide oxide mixture and prevent its high-temperature sintering into blocks, but also react with the carbide mixture to change the composition of the coating phase. Under vacuum conditions, the risk coefficient of graphitization of the diamond is relatively small. In the absence of other reactants, excess boron oxide is easily removed at the end of the reaction, enabling removal of the carbonized element with fewer impurities and reduced amounts of hazardous materials in the diamond. During the reaction, the surface temperature of the nanodiamonds should be maintained below 1100 °C. At that temperature, the surface morphology and chemical structure of the nanodiamonds change, although the diamond core remains intact[13].

Thus, in the present study, diamond nanoparticles and boron oxide were heated to a specified temperature under vacuum conditions, and held at that temperature for a period of time to complete the vacuum diffusion-deposition process of carbide particles on the surface of the diamond nanoparticles.

Boron oxide was mixed with nanodiamond in a B/C atomic ratio of 1:1. Plain nanodiamonds and the mixture were dried to remove moisture in a resistance furnace at 400~500 °C. After drying, each sample was moved to the vacuum system, heated to 500~1000 °C, and maintained at the final temperature for 10~40 min. The materials were then characterized.

XRD measurements of nanodiamond and its boron-doped product were obtained with a D/MAX 2400 X-ray diffractometer using a Cu Kα source with a scan speed of $1°·s^{-1}$. The elemental composition of the sample surface was analyzed by XPS. Raman spectra of the nanodiamond and its boron-doped product were obtained with a DXR Smart Raman spectrometer using the 532-nm line of an argon laser. The surface functional groups of the boride product were observed using a Shimadzu Fourier transform infrared spectroscopy

spectrometer. The microstructure of the boron-doped product was observed with a TecnaiG220 transmission electron microscope at FEI (USA). TG and differential thermal analyses (DTA) of the nanodiamond and its boron-doped product were obtained with a DSC822/TGA/SDTA851 at a speed of $1 °C·min^{-1}$.

2 Results and Discussion

2.1 TG and DTA results

TG and DTA were used to evaluate the thermal stability and oxidation resistance of the nanodiamond and boron-doped product via the onset of mass loss, the mass loss curve, and residual mass. Fig.1 shows the TG and DTA curves of the samples at different growth temperatures. The onset of mass loss for the raw material was calculated as 492.07 °C. The loss ends at 800 °C, leaving a residual mass of 13.8%. From the TG curve shown in Fig.1b, we estimate that the oxidation temperature of the boride product increases compared to that of the starting material by 175 °C to a maximum of 667.60 °C, and the product obtains a residual mass of 91.03% at 800 °C. The lowest residual mass of 68.34% was calculated for growth at 1150 °C. This suggests that the oxidation resistance of the product greatly increases. There is an obvious exothermic peak between 450 and 700 °C for the starting material in the DTA curve, as shown in Fig.1a. The oxidation rate of the boron-doped product is much slower than that of the nanodiamond. As expected, the presence of the carbide coating greatly reduces the oxidation rate of the nanodiamond and improves its thermal stability.
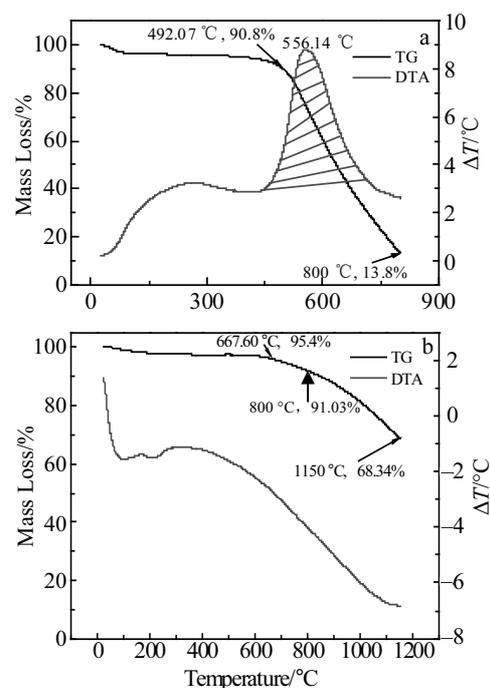

Fig.1   TG and DTA curves for nanodiamond (a) and 1:1 boron-doped product (b)

2.2 XPS analysis

Because the boron content in the boride product is very small (such that it exceeds the sensitivity of general elemental analysis equipment), XPS was used to assess the composition of the product (Fig.2). By calculating the integral intensities of the C 1s, O 1s, and B 1s spectra, the contents of the elements in the boride product were calculated (Table 1). The boron-doped product contains mostly carbon, a small amount of oxygen, and a much smaller percentage of boron.

2.3 X-ray diffraction analysis

Samples of the nanodiamond, nanodiamond heated to 1200 °C, and the boron-doped product were investigated by XRD. Fig.3 shows typical X-ray diffraction patterns for these samples, in which two main peaks from the nanodiamond are observed. The peaks at 43.916° and 75.303° can be indexed to the (111) and (220) planes of diamond, respectively. The diffraction peaks appear at similar positions for the samples, irrespective of treatment temperature. However, the intensity of the broad diffraction peak at 26° is reduced after heating.

The XRD pattern of the boron-doped product features broader peaks than those of the nanodiamond and heated nanodiamond. In addition, another peak appears at 40.145°, which is related to the boron-doped product and is different from the characteristic nanodiamond or heated nanodiamond peaks. The d-value of 0.225 nm determined from the XRD does not match the reported maximum number of Bragg peaks for boron carbide or boron oxide. This XRD peak instead indicates an obvious shift of the main peak of hexagonal diamond $(100)_D$, confirming that boron atoms were inserted into the nanodiamond[14]. The space group of the boron carbide or boric oxide species could not be determined from the XRD. The presence of a considerable amount of boron in the material indicates that boric oxides or boron carbide may be present as impurities.
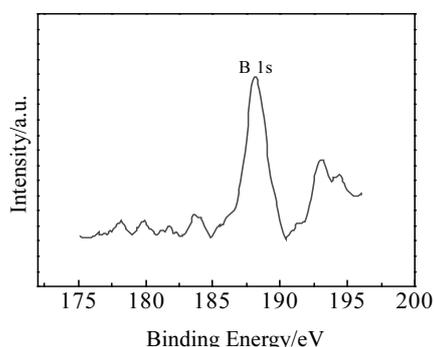

Fig.2 XPS spectrum of B 1s for boron-doped product

Table 1   Elemental analysis of boron-doped product

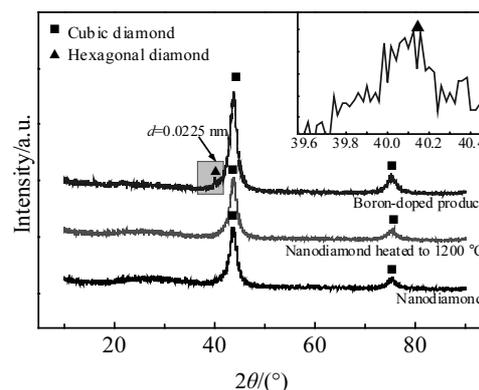| Element	C	O	B
Content/wt%	92.08	7.14	0.78

Fig.3 XRD patterns of nanodiamond, nanodiamond heated to 1200 °C, and boron-doped product

2.4 FTIR analysis

The functional groups of the nanodiamond, nanodiamond heated to 1200 °C, and boron-doped product were characterized by FTIR, as shown in Fig.4 and Table 2. Two states of boron are present in the nanodiamond, namely, substitutional boron atoms at 1324 cm^{-1} and interstitial boron atoms at 1451 cm^{-1}. Among these, the boron atoms substituted for carbon atoms form holes in the diamond and band overlap occurs, which enhances the conductivity of the diamond[15]. In the case of a low boron oxide content, boron atoms mainly exist in the form of substitutional carbon atoms and form C-B bonds in the diamond lattice. The bonds between two carbon atoms may be broken and replaced by C-O or C-B bonds. With the increasing concentration, the boron atoms can also enter lattice gaps and bond with impurities in the diamond (e.g., to form B–CH$_3$ and B–O bonds). The boron atoms which are inserted into the cubic structure of the nanodiamond may change the space group of the precursor. This change in bonding could explain the increase in lattice spacing from 0.219 nm to 0.225 nm.
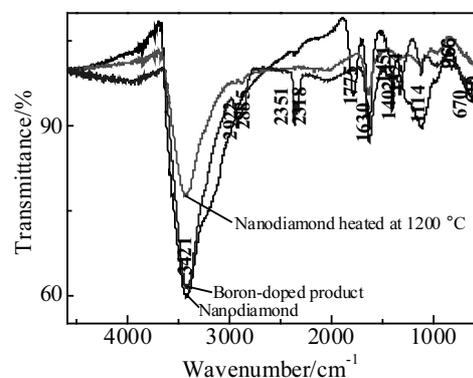

Fig.4 FTIR spectra of nanodiamond, nanodiamond heated at 1200 °C, and boron-doped product

Table 2　Functional group analysis of Fig.4

Functional group	Wavenumber/cm^{-1}	Functional group	Wavenumber/cm^{-1}
CO_2	2351, 2318	C–N	1402
–OH	1630, 3421	C–B	1324
C–C	2885, 2922	B–H	966
C=O	1775	B–N	610
C–OH	1114	B–O	670, 1451

2.5　Raman spectroscopy

Samples of the nanodiamond and the boron-doped product were subjected to Raman spectroscopy. In both Raman spectra, a broad absorption band is observed at 400~500 cm^{-1}; its intensity increases as the boron doping level increases (Fig.5). The peak at 1332 cm^{-1}corresponds to the sp^3 bonds of the nanodiamond[16]. The G peak at 1582 cm^{-1} is related to the relative movement of carbon atoms in a graphite plane, indicating sp^2 hybridization[17]. In detonation diamonds, the G peak has been reported to shift by 20 cm^{-1} to 1602 cm^{-1} because of the large amount of nitrogen which exists in the raw material used in the detonation process[18]. However, nitrogen doping cannot explain the G peak shift from 1608 cm^{-1} to 1620 cm^{-1} in our samples. The boron-doped product features the G peak, a D peak at 1331 cm^{-1}, and a shoulder at 1245 cm^{-1}. The G peak shift to 1620 cm^{-1} may be caused by residual graphite oxidation on the nanodiamond surface. Thus, doping boron atoms into the nanodiamond might increases the defects on the surface of the nanodiamond.

2.6　TEM analysis

As shown in Fig.6a, the shapes of nanodiamond particles are varied but easily distinguished. Most are approximately spherical, although irregular, with particle sizes of 2~10 nm. Compared with the nanodiamond, the diamond nanoparticles after boronizing are less distinct, although neither the diamond particle morphology nor their size is obviously changed. A small number of cubic diamonds are present. As shown in Fig.7a, high-resolution TEM measurements reveal a nanodiamond layer spacing of 2.067 nm (10 layer spacing). The
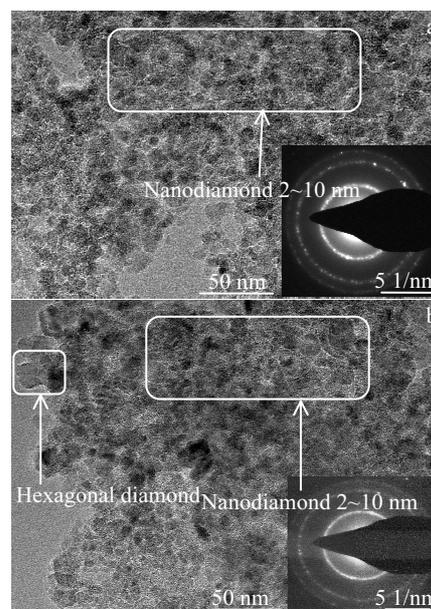

Fig.6　TEM images and SAED patterns of the nanodiamond (a) and boron-doped product (b)
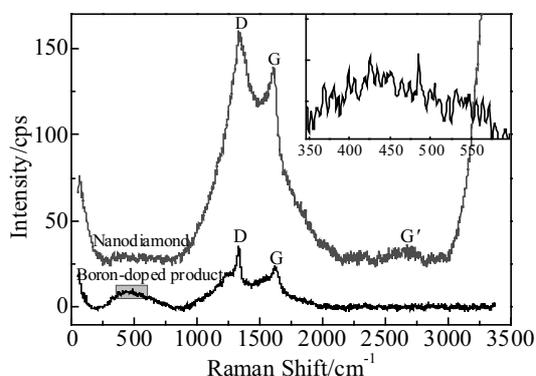

Fig.5　Raman spectra for the nanodiamond and boron-doped product
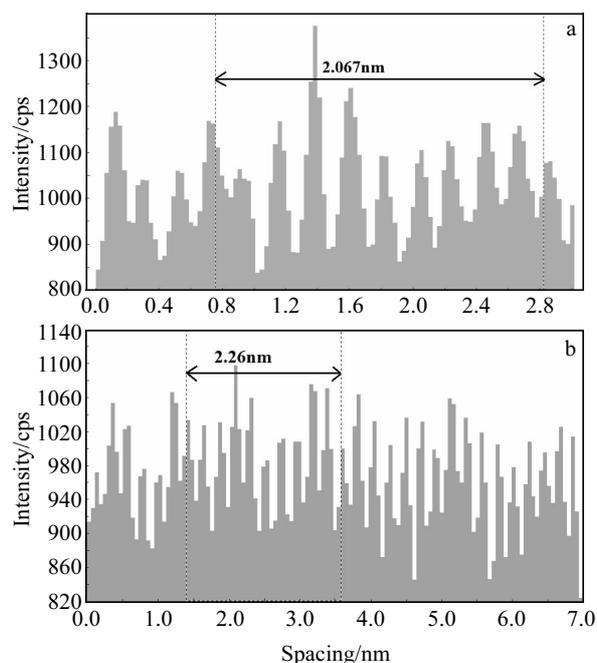

Fig.7　Interlayer spacings for the nanodiamond (111) plane (a) and hexagonal diamond (100) (b)

measurement result is 0.206 nm, which is consistent with the layer spacing of the diamond $(111)_D$ crystal surface, indicating that the observed carbon layer is the $(111)_D$ crystal surface of nanodiamond. The layer spacing shown in Fig.7b was obtained from the particle in the white box in Fig.6b. The calculated result for the 10-layer spacing is 2.26 nm, meaning that the layer spacing is 0.226 nm, which is consistent with the layer spacing of the hexagonal diamond $(100)_D$ crystal surface. In combination with Fig.3, it can be inferred that the observed carbon layer is the (100) crystal face of hexagonal diamond.

The process of diamond doped with boron can be considered as follows: (1) First, chemical bonds at the surface of the nanodiamond carbon clusters are broken. At this point, the energy required to form hexatomic cyclic graphite may be insufficient[19-21]. (2) As the temperature increases, boron oxide melts and vaporizes, breaking certain covalent bonds. (3) At a sufficiently high temperature, the free chemical bonds of boron oxide combine with σ bonds of the nanodiamond, generating new C-B and B-O bonds. The process of doping diamond with boron can be understood to involve the initial cleavage of chemical bonds on the surface of nanodiamond carbon clusters[22-25]. Carbon atoms in the lattice are substituted with boron, which enhances electrical conductivity. Boron incorporation also expands the lattice constants, especially above the semiconductor-metal transition. At high temperature in the vacuum system, polar bonds such as –OH, –COOH, –CHO, C–H, and –NH$_2$ on the surface of the nanodiamond are broken. B-O bonds are also broken, and B may recombine with the nanodiamond. The crystal structure of the nanodiamond appears to include contributions from graphite, as shown in Fig.5, indicating considerable changes to the nanodiamond structure.

3   Conclusions

1) The boron-doped nanodiamond mainly contains C, O, and B, with mass fractions of 92.08%, 7.14%, and 0.78%. In addition to diamond $(111)_D$ and $(220)_D$ diffraction peaks, hexagonal diamond $(100)_D$ diffraction peaks are also observed in the XRD pattern of the boron-doped product. The introduction of B atoms results in an increase in nanodiamond defects, causing the G peak to move to 1620 cm^{-1}. Boron atoms mainly exist in two forms: substitutes for carbon atoms in C-B bonds, or being bonded with impurity elements (e.g., B-O) in the diamond lattice. The shape and morphology of boron-doped nanodiamond particles exhibit no obvious changes from the pristine material. The particle size is 2~10 nm and a small amount of cubic diamond forms. In conclusion, compared to the starting nanodiamond, the initial oxidation temperature of the boron-doped product increases by 175 °C, its oxidation rate is slower, and its thermal stability is improved.

2) With the increasing temperature, the boron oxide melts, vaporizes, and undergoes boron covalent bond breakage.

Finally at a certain temperature, boron species with unsatisfying valences combine with the σ bonds of the nanodiamond to form new chemical bonds, including C-B and B-O linkages.

References

1   Ynsa M D, Ramos M A, Skukan N *et al*. *Nuclear Instruments and Methods in Physics Research Section B: Beam Interactions with Materials and Atoms*[J], 2015, 348: 174

2   Roy M, Dua A K, Nuwad J *et al*. *Journal of Applied Physics*[J], 2006, 100(12): 124 506

3   Gheeraert E, Gonon P, Deneuville A *et al*. *Diamond and Related Materials*[J], 1993, 2(5-7): 742

4   Gonon P, Gheeraert E, Deneuville A *et al*. *Journal of Applied Physics*[J], 1995, 78(12): 7059

5   Mondal S, Banthia A K. *Journal of the European Ceramic Society*[J], 2005, 25(2-3): 287

6   Nishimura K, Das K, Glass J T. *Journal of Applied Physics*[J], 1991, 69(5): 3142

7   Kaner R B, Kouvetakis J, Warble C E *et al*. *Materials Research Bulletin*[J], 1987, 22(3): 399

8   Kowbel W, Huang Y, Huan K W. *New Carbon Materials*[J], 1995(1): 31 (in Chinese)

9   Paprocki K, Fabisiak K, Bogdanowicz R *et al*. *Journal of Materials Science*[J], 2017, 52(17): 10 119

10   Li Chunyan. *Thesis for Doctorate*[D]. Changchun: Jilin University, 2006 (in Chinese)

11   Zang Jianbing, Huang Hao, Zhao Yucheng. *Diamond & Abrasives Engineering*[J], 2002(1): 16 (in Chinese)

12   Rao T N, Fujishima A. *Diamond and Related Materials*[J], 2000, 9(3-6): 384

13   Xu Xiangyang, Zhu Yongwei, Wang Baichun *et al*. *Journal of Materials Science and Technology*[J], 2005, 21(1): 109

14   Ushizawa K, Watanabe K, Ando T *et al*. *Diamond and Related Materials*[J], 1998, 7(11-12): 1719

15   Huang Hao. *Thesis for Master*[D]. Qinhuangdao: Yanshan University, 2004 (in Chinese)

16   Ferreira N G, Abramof E, Corat E J *et al*. *Diamond and Related Materials*[J], 2001, 10(3-7): 750

17   Goncalves J A N, Sandonato G M, Iha K. *Diamond and Related Materials*[J], 2002, 11(8): 1578

18   Pruvost F, Bustarret E, Deneuville A. *Diamond and Related Materials*[J], 2000, 9(3-6): 295

19   Salzmann C G, Murray B J, Shephard J J. *Diamond and Related Materials*[J], 2015, 59: 69

20   Zhuang H, Yang N J, Fu H Y *et al*. *ACS Applied Materials & Interfaces*[J], 2015, 7(9): 5384

21   Ferrari A C, Robertson J. *Philosophical Transactions of the Royal Society of London A: Mathematical, Physical and Engineering Sciences*[J], 2004, 362(1824): 2477

22   Lee G D, Wang C Z, Yu J *et al*. *Physical Review Letters*[J], 2003, 91(26): 265 701

23　Jiang Q, Li J C, Wilde G. *Journal of Physics: Condensed Matter*[J], 2000, 12(26): 5623

24　Pantea C, Qian J, Voronin G A *et al*. *Journal of Applied Physics*[J],

2002, 91(4): 1957

25　Dabscheck B. *Journal of Industrial Relations*[J], 2016, 58(1): 150

硼掺杂纳米金刚石的制备及表征

严仙荣 [1]，李晓杰 [1,2]，王小红 [1,2]，闫鸿浩 [1,2]

(1. 大连理工大学，辽宁 大连 116024)

(2. 工业装备结构分析国家重点实验室，辽宁 大连 116024)

摘　要：采用高温真空扩散法制备了硼掺杂纳米金刚石。采用热重分析仪、X 射线光电子能谱仪、X 射线衍射仪、傅里叶变换红外光谱仪、智能型拉曼光谱仪、透射电子显微电镜等技术手段对制备的产物进行表征。结果表明，产物主要包含 C、O、B 元素，其质量分数分别为 92.08%，7.14%，0.78%。硼掺杂纳米金刚石的 XRD 图谱中除了金刚石$(111)_D$、$(220)_D$ 衍射峰外，还有六方金刚石$(100)_D$ 的衍射峰。B 原子的引入造成纳米金刚石的缺陷增多，引起 G 峰移至 1620 cm^{-1}。硼原子在金刚石中以 2 种状态存在，分别是 C-B 碳的取代原子和 B-O 的间隙硼原子。掺杂后的纳米金刚石颗粒形状和形貌无明显变化（爆轰纳米金刚石的粒径 2~10 nm），有少部分立方金刚石的存在。总而言之，硼的掺杂使得纳米金刚石的初始氧化温度提高了 175 ℃，氧化速度缓慢，热稳定性能提高。

关键词：硼掺杂纳米金刚石；抗氧化性能；热稳定性；高温真空扩散法

作者简介：严仙荣，女，1970 年生，博士生，大连理工大学工程力学系，辽宁 大连 116024，E-mail: yxr5ok@163.com